63-3-I

ASD TR 61-436
PART I

NONDESTRUCTIVE ANALYSIS OF THE BRITTLE FRACTURE BEHAVIOR OF CERAMIC MATERIALS

TECHNICAL REPORT NO ASD TR 61-436, PART I

February 1963

DIRECTORATE OF MATERIALS AND PROCESSES
AERONAUTICAL SYSTEMS DIVISION
AIR FORCE SYSTEMS COMMAND
WRIGHT-PATTERSON AIR FORCE BASE, OHIO

Project No. 7360, Task No. 736002

(Prepared under Contract No. AF 33(616)-7347
by Mississippi State University, State College, Miss.
J. H. Lauchner, T. F. Torries, J. L. Pentecost, authors.)

$5.00

NOTICES

When Government drawings, specifications, or other data are used for any purpose other than in connection with a definitely related Government procurement operation, the United States Government thereby incurs no responsibility nor any obligation whatsoever; and the fact that the Government may have formulated, furnished, or in any way supplied the said drawings, specifications, or other data, is not to be regarded by implication or otherwise as in any manner licensing the holder or any other person or corporation, or conveying any rights or permission to manufacture, use, or sell any patented invention that may in any way be related thereto.

Qualified requesters may obtain copies of this report from the Armed Services Technical Information Agency, (ASTIA), Arlington Hall Station, Arlington 12, Virginia.

This report has been released to the Office of Technical Services, U.S. Department of Commerce, Washington 25, D.C., in stock quantities for sale to the general public.

Copies of this report should not be returned to the Aeronautical Systems Division unless return is required by security considerations, contractual obligations, or notice on a specific document.

24-565C, 600, 4-11-63

FOREWORD

This report was prepared in the Department of Ceramic Engineering at Mississippi State University under USAF Contract No. AF 33(616)-7347. This contract was initiated under Project No. 7360, Task No.736002. It was administered under the direction of the Directorate of Materials and Processes, Deputy for Technology, Aeronautical Systems Division, with Mr. Richard R. Rowand acting as Project Engineer.

This report covers the period of work from September 1, 1960 to August 31, 1961.

Personnel participating in the research included Julian H. Lauchner, principal investigator, Joseph L. Pentecost, Thomas F. Torries, Robert E. Reed and James A. Scarborough.

ABSTRACT

A literature survey of theoretical and experimental approaches to brittle fracture was directed toward a nondestructive evaluation point of view. Surface decorating techniques were investigated.

A technique for calculating maximum stress in an elastic loop was developed and applied to the measurement of the strength of glass fibers from three to seven mils in diameter. The strength values were related to surface condition by surface decoration techniques. Surface flaw decoration of cleaned and polished surfaces was performed by condensation of water on the surface. Minute flaws estimated to be less than 1000 Å deep were easily revealed.

Capacitance behaviors of polycrystalline materials were studied. Residual stress effects were observed under statically loaded conditions.

This report has been reviewed and is approved.

W. J. TRAPP
Chief, Strength and Dynamics Branch
Metals and Ceramics Laboratory
Directorate of Materials and Processes

TABLE OF CONTENTS

LIST OF ILLUSTRATIONS

LIST OF ILLUSTRATIONS (Cont'd)

I. INTRODUCTION

The high temperature strength and corrosion resistance of many readily available polycrystalline, inorganic materials are generally recognized. It is because of this that they should be, and indeed are being, given serious consideration for structural use in zones of high temperature and stress. The most serious deterrant to their use, however, is a characteristic brittleness.

From a space travel point of view, cases exist where an improvement in the strength behavior of ceramic, cermet, and graphite materials is needed, but in many cases, a more critical interpretation of the serviceability of these materials is a prerequisite to component performance.

As the result of higher stresses, load factors, and service temperatures encountered in space travel, component reliability has come to be a must in engineering design.

Until recent years the designer has always been able to depend upon inelastic deformation as a means of correction for unforseen environmental conditions. The performance targets of today, however, place demands upon the designer as well as the materials which leave little tolerance. For this reason, the subject on nondestructive evaluation has come to mean more than component performance prediction. A real need now exists for concepts of material behavior which will form the basis of new design philosophies and nondestructive concepts of material performance.

The phenomena of inelastic deformation and brittle fracture exhibited by multi-phase as well as single phase, inorganic, nonmetallic materials are currently receiving extensive theoretical and experimental analyses from the macrostructure as well as the microstructure points of view. Grain size, orientation, particle packing, structural dislocations, residual stress, and surface imperfections have been employed in fracture mechanism concepts. Present knowledge and techniques have progressed to the point that it is possible to appreciate the mechanical behavior of crystalline composites. Unfortunately, however, our understanding of flow and fracture of these materials is so rudimentary that only qualitative predictions are as yet possible.

These phenomena must be carefully considered before any really significant nondestructive tests of ceramic, cermet, and graphite materials can be evolved.

The research program of Air Force Contract AF 33(616)-7347 was directed toward furthering the understanding of brittle fracture behavior of ceramic, cermet, and graphite materials with the ultimate goal of evolving nondestructive performance evaluation techniques based upon fundamental concepts. The research work

Manuscript released by the authors August 1962 for publication as an ASD Technical Report.

was performed in the newly established Department of Ceramic Engineering of Mississippi State University.

II. THEORETICAL AND EXPERIMENTAL BACKGROUND

The strength of brittle materials has been treated by many investigators.[1-18] One of the early investigators who has been frequently referenced with Griffith who attempted to explain the difference between the theoretically derived strength of glass (about 1.5×10^6 psi) and that experimentally determined (about 10^4 psi) by the postulated existence of microscopic flaws in the surface with crack tip dimensions approaching atomistic dimensions.[18] Griffith's concept of flaws and their dimensions has withstood the test of time and even current literature references these "flaws" in attempting to explain the brittle behavior of many materials.

Many attempts have been made to observe the flaws postulated by Griffith or to develop flaws of similar dimensions under controlled conditions.[2,19,13] Those investigations have generally concurred with Griffith's hypothesis; the radius of the crack tip, the size of the flaws, the number per cm^2 of surface, and other surface properties have been reported.[9] While this concept has proven useful, attempts to observe directly the Griffith flaws or to decorate these flaws for observation by thin layers of absorbed or condensed phases have been reported.[2,19,20] The most common of these are the "breath figures" caused by condensation of the moisture from the breath and the observation of these figures. Other attempts at etching and recrystallization have also been reported.[13,21,22,23] Some interesting photomicrographs of surfaces have been published strengthening the flaw hypothesis.

The effect of surface preparation in any study of brittle materials is of prime concern. Immobility surface ions in solids as compared to liquids, has hampered, in many cases, the preparation of suitable surfaces for study.[24] Ordinary surfaces are uneven and difficult to clean. Polished surfaces are invariably disturbed, covered to some degree with a layer of amorphous material. For glass and some inorganic crystals, the depth of this disturbed layer may extend to 3000 Å below the surface.[24]. Controversy exists, but experimental data has been presented to support the hypothesis of surface melting or flow in any polishing operation involving mechanical working. Electropolishing, flame polishing, and cathode sputtering, among other techniques have been used to overcome some of these obstacles.

The origin of the Griffith flaws and their development under various environmental conditions, has been the subject of many investigations. Griffith proposed the spontaneous generation of these "flaws" by variations in composition resulting between groups of more highly ordered atoms. This might be called a type of "micel" theory, where the flaws occur between small individual micels, each micel having more or less internal order. The efforts of these individual micels to orient their constituent atoms was postulated to generate the internal stresses

which spontaneously caused flaw development. The minute changes in the volume of glass at room temperature shortly after forming was presented as supporting evidence. The tensile strength decrease of fibers after drawing was also quoted in support of this hypothesis.

Other explanations for the development of flaws have included atmospheric attack by water vapor and the difference in surface glass compositions compared to glass not exposed to the atmosphere.[25, 26, 21]

While the Griffith flaw theory was used for many years to explain the differences in tensile strength of glass in the bulk and fiber condition, Otto showed that the temperature of drawing the fiber and other parameters could explain tensile strength variations with diameter.[1] Since no "molecular" orientation has been observed in glass fibers, other means of explaining the strength in fibrous form are obviously necessary.[27]

The relationship of the mechanical properties of glass to its surface state requires further understanding. The importance of glass, in general, to ceramic materials is readily apparent when it is considered as a major constituent of many porcelains and other materials;[8] as the "impurity" in many so-called pure oxide materials, and as the artifact resulting from the liquid phase formed in sintering many polycrystalline ceramic materials.

The importance of glass in a typical porcelain is widened by Mattyasovsgky's work on glass-crystalline composites.[8] He found that contrary to popular belief, the mullite needles in typical porcelains were not the contributor of high strength, but that the glassy matrix and the resulting internal stress caused by the thermal expansion of the glassy matrix was the primary factor controlling mechanical strength. It was shown that quartz included in the glass matrix to increase its effective thermal expansion would improve the mechanical strength of the porcelain. Other work on microstresses in multiphase systems has shown the importance of the thermal expansion and resultant internal stresses on material properties.[28, 29, 30, 31] The importance of the grain boundary (and the glass in the boundary) in inducing or preventing slip in polycrystalline ceramics has been reported.[32] The decrease in mechanical strength at elevated temperatures has been postulated due to grain boundary slip. The relationship between the stress system and the measured yield in "brittle" materials has been indicated by recent micro-hardness measurements.[10, 33, 34, 35] Several investigators feel that if high compressive stresses could be induced perpendicular to the applied tensile stress, marked ductility would result. Microhardness (indentation) measurements on both glassy and crystalline materials have been used to support this theory.

Recent work in ductility of single crystal oxide materials is also closely related to the understanding of brittle fracture. It has been shown by Gorum et al

and May that many single crystal oxides exhibit the same kind of deformation mechanism as metals and that these mechanisms may be effective at room temperature.[9,23,21,22] The relation of impurities and heat treatment has shown the analogous behavior of oxides and metals. Impurities in solution at elevated temperatures, quenched to room temperature do not impair ductility as when precipitated by slow cooling. The dependence of critically resolved shear stress on the impurity content and heat treatment has been explained by solution-precipitation of the impurities.

With crystals, the study of deformation mechanisms and submicroscopic structural inhomogenity or lattice deformation has been enhanced by the development of techniques for "decorating" dislocations and various "flaws" or imperfections. Theoretical explanations have thus been verified by experimental observations.

Recent contributions in the field of failure of ionic[47] crystals and graphite[48] indicate that "flaw" decoration techniques are still the basis for obtaining information by which structural mechanisms can be postulated and proven. The concept of a "flaw" in a brittle material may be extended to include bonding irregularities, compositional irregularities at the atomic level or microscopic cracks and surface defects. The engineering approaches[49,50,51] to the use of Griffith-Irwin fracture mechanics and Neuber's stress concentration concepts were compared and found in reasonable agreement.

III. EXPERIMENTAL APPROACH

A. Flaw Decoration

Among the tools for understanding properties of solids, flaw decoration techniques have been the basis for many important discoveries or confirmations. Early in the program for the development of techniques for studying brittle fracture, it was felt that any methods which would allow the study of actual surface conditions as related to surface treatments would be helpful in studying brittle fracture. Though many attempts have been made to observe Griffith flaws by electron microscope and other decoration techniques, to date little conclusive and definite visual proof has been presented.

Perhaps the concept of "flaw" is not accurate; the "flaw" in a glass surface might be compositional inhomogenity, bonding irregularity or bond orientation discrepancies. Whatever the cause or mechanism, the decoration and observation of these critical areas is of prime importance in any study of brittle fracture.

If "flaws" or any inhomogenity exists, there must be an accompanying local variation in the surface energy and hence, under proper conditions, decoration of the locations of high energy should be possible.

In analyzing the difficulties that have been met by other investigators, it is obvious that the definition of surface state is of prime importance. Freshly cleaned, fire polished and annealed surfaces should represent the nearest approach to surface perfection in glass. If these heating processes could be performed in vacuo, further improvement might be expected. Etching, absorption, recrystallization and diffusion decoration techniques for such surfaces should show marked differences when compared to surfaces prepared by washing, polishing or etching. The latter processes disturb the surface sufficiently to mask many of the effects which might be inherently present.

While glass leads itself well to this study, the surfaces of any "brittle" material could be used. The surface of mica, for example, is unique in that no cleaning would be required because a fresh surface could be cleaned when desired. Such a material should exhibit near perfect surface cleanness. Decoration of damage to a mica surface would constitute one step in studying flaw decoration since surface cleanness could be eliminated as a variable.

The objective of any surface "decorating" project should be the correlation of observed results with measured properties, and in this case glass samples must ultimately be broken and strength values measured. Stress levels should correlate well with values calculated from the observed data.

The thin rods or fibers of glass can be used to illustrate the change occurring on fiber surface. When bent into a tight loop, a freshly drawn fiber can be stressed much more highly than when it has aged. Loops of fresh glass fibers, highly stressed by the small radius of curvative, break spontaneously after the fibers stand in normal air for a short period. Obvious changes occur in the fiber and the surface character is normally blamed for this change. If the surface "appearance" can be correlated to observed strength, then a nondestructive test may be practical.

Experimentally, the observation of surface defects is most important. The absorption of radioactive ions and the autoradiograph of the surface to reveal "flaw" sites appears to be a promising decoration approach.

Other experimental methods for flaw observation include "breath figures" produced by condensing moisture on a clean glass surface and observing these patterns through the microscope. Evidence has been presented that this technique will decorate flaws, however, the cleaning of the surface disturbs a thin layer on the solid and the influence of this layer on the observed results has not been established. The "flaws" observed could be artifacts of the polishing operation and this possibility must be eliminated conclusively.

According to many investigators who have used the flaw hypothesis, the surface flaws can be healed by proper heat or chemical treatment. The international development and healing of such "flaws" must be revealed by the decoration method if conclusive evidence of the surface state is to be presented.

Efforts were concentrated on correlating observed strength characteristics with surface conditions. Both the problems of adequate strength measurements and "flaw" decoration techniques were encountered. Glass fibers were successfully prepared under a number of conditions and strength measurements made. Breath, or vapor patterns, as used by Levengood[52] were repeated successfully, and this work extended to include fire-polished surfaces and other surface treatments.

In preparing "fresh" fibers, large discrepancies in strength values have been observed. There is some evidence that freshly drawn fibers less than one minute old exhibit much lower strengths than those several minutes old, while further atmospheric exposure causes a decrease in strength. This early low strength phenomea has not been previously reported and this was possibly due to the short time period required to prepare and break a loop compared to other strength measuring techniques. It should be emphasized that these results are limited.

Various cleaning methods were sought in the vapor or "breath" pattern study. The formation of breath patterns has proved to be an interesting technique to pursue. By using a specially prepared petri dish with a cover containing two holes, one over which the specimen was placed and the other opened at will to control condensation, excellent control of the patterns was possible.

The finest grade of polishing alumina, (gamma alumina less than 0.1 particles) when used for cleaning or polishing glass surfaces leaves a scratch pattern easily revealed by vapor patterns, although the scratches are not visible under ordinary high-power optical examination.

The use of a "flame polishing" technique (actually only heating and cooling of the cleaned and washed surface) causes the surface "flaws" to heal so that no pattern is detected upon examination. This technique for cleaning the surface is applicable to cleaning fibers just prior to breaking so that the strength characteristics can be compared with the surface characteristics.

B. Internal Structure

As the work on this program developed, it became apparent that two avenues for investigation of brittle fracture should be pursued. First, the surface contributions to the development of the fracture development and second, the contribution of internal stresses, internal flaws, or "bulk" effects. In the discussions which follow, the relation of the studies to each of these areas is outlined.

To study internal stresses in brittle materials, the change in dielectric constant with stress was determined. Internal stress results in the permittivity anisotropy measurable as a change in dielectric constant, if sufficiently sensitive measuring techniques can be devised. Internal stress patterns in glasses and transparent materials have been frequently determined by the use of polarized light. The measurement of dielectric constant should yield similar data since polarized light depends on variations in index of refraction with stress, and the index of refraction and dielectric constant are related:

$$K = n^2$$

K = dielectric constant) both measured at the same
n = index of refraction) frequency

IV. EXPERIMENTAL EQUIPMENT AND TECHNIQUES

A. Surface Imperfection Studies

Initial work with glass fibers was performed with fibers drawn from the reduction of a glass rod. This technique produced fibers, but the uniformity achievable was not satisfactory for making loops, since the variation in fiber diameter resulted in unsymetrical loops. For such loops, the stresses are difficult to calculate because the radius of curvature of the fiber is difficult to measure.

By melting clean glass rod in a crucible, allowing the air bubbles to fine out and lowering the temperature until the glass became viscous, fibers could be drawn which were of uniform diameter for 6 or 8 feet. By adjusting the glass temperature, and controlling the drawing rate, fibers of any desired diameter could be drawn. After drawing, fibers were cut, one end placed in holes in a refractory brick and annealed. Care was taken to assure that only the ends of the fibers were touched during the cutting and annealing.

Several methods of forming loops were tried. For large fibers, about 10 mils in diameter, the ends of each fiber were placed in two vertical holes in a wooden block several cm apart, the distance between holes determining the stress level in the fiber.

For smaller fibers, L-shaped loops were made by crossing the fibers ends and cementing in place. By making the intersections at 90° and measuring either the height of the loop or the length of the fiber in the loop, and the fiber diameter, the stress level in the fiber was easily calculated. Fibers produced by these techniques and dipped in radioactive isotope solutions were autoradiographed by placing the dried fiber in contact with type "M" X-ray film. By folding the film

and placing the small fiber in the fold, about 270° of the fiber's circumference could be radiographed. By observing the radiograph under the microscope, the concentration and location of the isotope could be determined.

Efforts were concentrated on "breath figures" for decorating the flaws on flat glass surfaces. By cleaning thoroughly a glass slide or cover slip using the procedure outlined by Levengood, glass surfaces were decorated with breath figures. To produce a breath figure, the cleaned glass surface is cooled by dipping in rinse water, blown dry with a light air blast, and moisture from the breath is condensed on the surface. Immediately a cover slip with a thin, rectangular ring rubber cemented around the edge is placed over the surface to prevent evaporation. The cover slip must be slightly warmer than the surface on which the moisture is condensed to prevent condensation on the lower side of the cover slip.

Difficulties were encountered in initial observation because the working distance between the objective lens and the decorated surface was only about 0.3mm. This allowed only a small distance in which to make a cover glass and seal. The application of a sufficiently thin rubber gasket to cover slip presented some difficulty, but a small square of a rubber balloon was finally cemented to a 150 thick cover glass. The center of the rubber square was carefully cut with a razor blade and pealed out, leaving a ring-shaped gasket capable of sealing on a flat glass surface.

Random patterns similar to those reported by Levengood were observed on freshly cleaned and polished surfaces. On ordinary surfaces, not polished, the "flaw lines" attributed by Levengood to Griffith, flaws were observed.

B. Dielectric Studies

Specimens of .020 alumina made by the American Lava Corp. were used for investigation of loading effects on alumina and the variation in electrical properties.

An intensive search for suitable measuring equipment revealed the ESI Bridge with a resolution of .001 pfd up to 100 pfd, and this seemed adequate for this investigation. Samples were initially prepared by applying fired silver electrodes in a precise area on both surfaces. About 1 cm^2 was used for electrode area and yielded about 35 pfd capacitance.

Efforts to load these specimens in compression always resulted in fracture below 15,000 psi, due to surface unevenness and the resultant bending stresses introduced. Various techniques were used to alleviate this, but the use of paper gaskets, metal foil gaskets, hard rubber plattens, and plastic gaskets all proved unsatisfactory. Polishing the surface of the fired silver electrode until flat was tried unsuccessfully. Initial data was promising, but no measure of reproducibility

and accuracy could be made until more satisfactory loading arrangements had been achieved.

Two 1/2" thick 2" X 2" mild steel plates were then polished flat over the center area rising 20 grit abrasive on a flat glass plate and later between the two plates. The center section was then cut from one plate (about 1/3 $in.^2$) and an alumina specimen slightly smaller than the plate was placed between the two plates, using a film of oil for lubrication. Leads were attached to the two steel plates, and these were insulated from the press frame with an alumina block and transite sheets.

With this arrangement, the alumina could be loaded up to 50,000 psi without difficulty, further load to the point of deforming the blocks has been used satisfactorily, but for pressures higher than 50,000 psi, harder surfaces are needed to apply the pressure.

C. Experimental Apparatus

The construction of a device for forming a loop in a fiber and decreasing the loop until failure is shown in Figure 1. The device consists of a micrometer movement attached to a small table which slides in guides to maintain straight line movement without tilting. On the table is the lower clamp assembly to hold one end of the fiber vertically. Above the movable table is a fixed table with a hole through which the vertical end of the fiber passes. The fixed table contains the second clamp assembly which clamps the other end of the fiber horizontally, forming a loop with the ends intersecting at 90°.

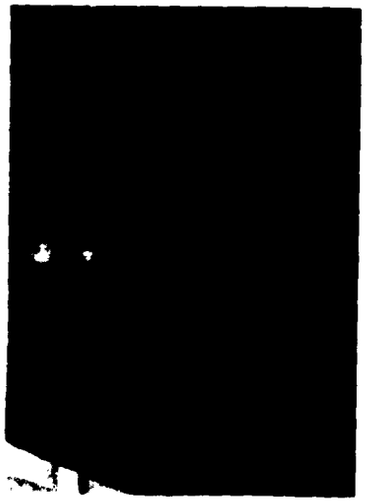

Figure 1. Device for forming and breaking glass fiber loop.

To use the loop device, it is either necessary to mark off a predetermined distance on the fiber using two dots of ink from a beam compass with two marking points, or to measure the remnants of the loop after failure. If the fiber is marked, the fiber is loaded and adjusted so that the two marks coincide at the loop intersection and the micrometer is read. After lowering the movable table and decreasing the loop length until failure, the micrometer is again read. The difference in micrometer readings is substracted from the marked length to obtain loop length.

When no marking is used, a small scale is used to measure each end which remains after loop failure. These two measurements are added to obtain loop length at failure.

Both loop length measuring techniques have proven satisfactory and provide sufficient accuracy considering possible errors due to fiber ellipsicity, diameter, uniformity, and accuracy in measuring the fiber diameter uniformity, and accuracy in measuring the fiber diameter .

Figure 2 shows the petrographic microscope and special petri dish used for breath or vapor pattern observations. The bottom of the petri dish is covered with warm water, the specimen is mounted on the top of the petri dish, cleaned side down. The top is placed over the petri dish and the microscope focused on the lower (cleaned) surface of the glass specimen. A vapor pattern from condensation begins to form rapidly and can be regulated by water temperature and opening or closing a second hold in the petri dish top. Best observations occur early in the pattern formation when the droplets are small and the "flaws" on the surface act as nuclei for condensation. A vapor pattern can be maintained for 3 to 10 minutes with little difficulty.

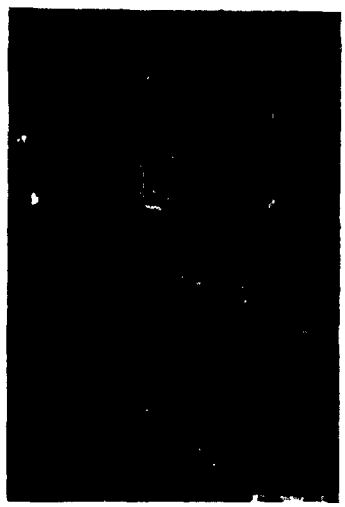

Figure 2. Petrographic microscope with petri dish and accessories for obtaining vapor patterns. The camera has been removed for this picture.

For the observation of the "decoration" techniques, a Leitz Ortholux microscope. Figure 3, was employed. The versatility of this instrument in illumination, vertical, transmitted, dark field, etc., and the quality of the optics enhanced observations.

For stressing the glass slides while etching and for applying bending stresses to the alumina bars for dielectric measurements, a small loading device shown in Figure 4 was constructed. The small furnace used with the loading jig is shown in Figure 5. The loading device was constructed so that it could be inverted to maintain a fluid on either surface of the glass slide. For stimultaneous etching of both surfaces, one drop "hangs" by surface tension from the lower surface.

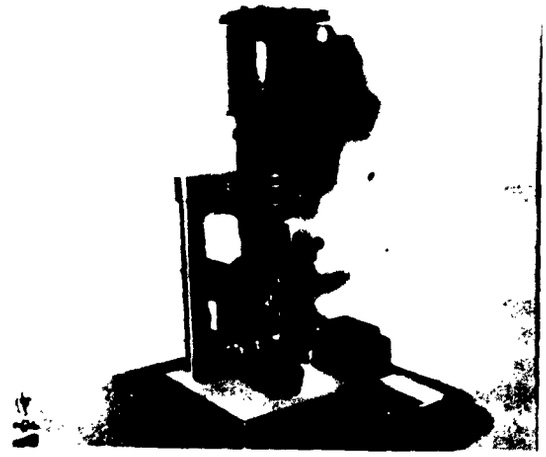

Figure 3. Metallographic-Petrographic Microscope

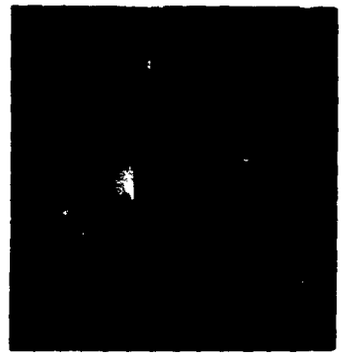

Figure 4. Loading Jig

Figure 5. Heat Treating Furnace

V. EXPERIMENTAL RESULTS

A. Surface Imperfections

Fiber strength measurements of soda lime glass fibers 3-7 mils hand pulled from a rod indicate average strengths of 120,000 psi with a standard deviation of 27,000 psi. These fibers were less than six hours old and all measurements were made on the device described in the previous section. The variation in strengths can probably be largely attributed to the temperature of the glass before pulling and the quenching rate.

The same fibers as prepared above, but aged for three days exhibited average strengths of 60,000 psi with a standard deviation of 11,000.

Fibers broken by hand by rapidly forming a loop, tightening the loop until failure and measuring the remaining loop sections exhibited strengths of 62,000 psi with a standard deviation of 12,000 psi. All measurements were made within 30 seconds of forming the fiber.

The attack of normal atmosphere on the surface of a freshly drawn glass fiber was easily shown by drawing tight loops of fresh glass fibers. In the "virgin" condition, the strength of these fibers is comparatively high; their ability to withstand 200,000 psi tensile stresses was not uncommon as shown in Appendix I. After preparing a small loop with 100,000-150,000 psi tension in the loop, cementing the ends of the loop and leaving the loop in air, the loops broke spontaneously when the condition of the glass surface changes and the strength dropped below the stress level in the loop. Maximum stress calculations were based on the nomogram shown in Appendix II.

When fibers were bent into a tight loop, the fiber ends crossed and cemented, exposure to normal air caused fracture within 24 hours in 90 per cent of the samples.

More careful attention to radius of curvature and fiber uniformity should have increased the uniformity of these determinations.

In the early attempts to decorate flaws on glass surfaces in this contract, the work of Levengood[52] was repeated with good results. Water vapor condensation revealed flaw characteristics, but the experimental technique was difficult to apply to fibers and curved surfaces, and the observations were frequently rather transient.

While these patterns confirm Levengood's work, the question concerning the effect of the amorphous layer (due to polishing) remains. A basis for further surface decoration and preparation studies was laid by some preliminary work on freshly cleaned mica surfaces. Since mica presents an extremely clean surface

immediately after cleaving, the same sample may be viewed after several treatments by peeling successive layers, it was selected as a representative crystal surface. In natural mica the shifting of formations frequently stresses the crystals sufficiently to cause slip distortion, internal stresses and flaws. These must be considered when selecting a specimen for study. In the mica used in this study, minute flaws were observed parallel to the axes of the crystal. Throughout the crystal, however, these flaws were sufficiently far apart not to interfere with other observations and provide some "natural" flaws to decorate. In noting these flaws, it could be seen that they are often not continuous through the crystal and often terminate below the cleaved surface, providing disturbed areas above the cleaved surface.

Mica surfaces damaged by the point of a scribe show a six point "Star" with the lines following the A axes of the crystal. When the visibly damaged layers are peeled away, the damage can be again revealed by a breath pattern on the fresh surface. Similarly, a 2 per cent solution of sodium chloride can be carefully dried to form small crystals on the fresh surface revealing the damaged area. These techniques for studying surface damage show promise in revealing the actual nature of the change occurring on fresh glass surfaces.

Comparison of the etching process developed by Levengood[52] and the $LiNO_3$-KNO_3 diffusion process and their ability to reveal "flaws" on glass surfaces was made. The $LiNO_3$-KNO_3 diffusion caused a crack pattern on the surface influenced by the internal and external stresses in the glass. The NaF-HCl etch revealed surface damage and scratches not visible by other techniques.

Typical results from the breath or vapor pattern studies are shown in Figure 6 and 7. Figure 6 shows a cleaned surface as prepared by Levengood's[52] technique; Figure 7a shows a similarly cleaned surface which has fine scratches from a polishing with gamma alumina, the scratches are estimated less than 0.1μ deep. Figure 7b shows the same surface after flame polishing. Difficulties in reproducing the required detail in the photomicrographs from this study preclude the use of extensive illustrations in this report. Much of the observation of the vapor patterns is a transient observation progressively changed in detail and clarity.

The NaF -HCl etch used by Levengood[52] was found to reveal surface flaws and scratches vividly in most cases. Cleaned microscope slides showed a residual pattern from some flaws induced in manufacture. The pattern was irregularly-spaced parallel lines of narrow width, less than 10μ, which traversed the short dimension of the slide. These lines were present on all slides prepared by NaF -HCl etch, regardless of etch time, (assuming sufficient etch time was given to reveal the lines initially). In appearance, the lines seem to have minute depth.

Figure 6. Vapor Patterns

(a)
Washed, cleaned with precipitated calcium carbonate. Note small horizonal flaw.

(b)
Washed, cleaned with precipitated calcium carbonate. A different area on (a).

Figure 7. Vapor Patterns

(a)
Washed, cleaned with precipitated calcium carbonate, and polished (horizontal strokes) with 0.1 gamma alumina.

(b)
Same surface as (a) after heating to 1000°C and cooling. No pattern is visible.

Scratches produced by No. 1 levigated alumina polishing on the surface of the glass could be easily revealed by NaF-HCl etch. For the finer alumina, (Gammal) where the particles were less than 1000A, and hence the scratches, generally less than that depth, difficulty was encountered in revealing the scratches conclusively. The possibility always exists of a chance large grain contaminating the fine alumina and the patterns observed always showed some large scratches. The etching time for optimum definition also seemed critical with very fine flaws and must be varied to achieve best results.

Much time was spent in studying the "decorating" by $LiNO_3$-KNO_3 diffusion on the glass surface. If a clean uniform glass surface is "etched" (diffused), a fine, shallow surface crack pattern develops in which the number of cracks is proportional to the diffusion time. When examined, this pattern shows little organization, but a sequence of crack formations can be postulated from their intersections just as shown by Gordon, Marsh et al.[53]

If, however, a small stone is encountered at the surface, the flaw pattern will emphasize this flaw by local crack arrangement, Figure 8.

For glass surfaces under tension or compression, quite different results are obtained. In trying to emphasize the effects of surface flaws by "opening" them in tension, a series of samples were prepared, etched while under about 80 per cent of the breaking stress.

On the tensile side, the cracks were roughly parallel and ran perpendicular to the tension direction. Where a single crack deviated from this parallel pattern, a "flaw" was interpreted as being present. The deviation of a series of parallel lines in a similar fashion in a given area outlined a "defect" vividly; this is illustrated in Figure 9.

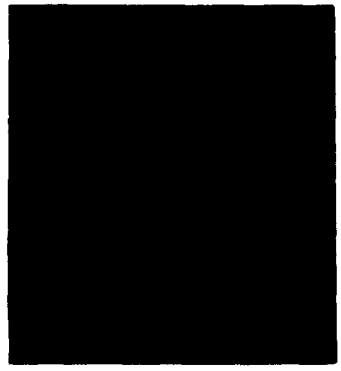

Figure 8. Inclusion Fracture Morphology

Figure 9. Tensile Fracture Discontinuities

By applying tensile stresses again at room temperature, in the same direction as applied during etching, the crack pattern could be "opened" showing that the etching surface was essentially in compression at room temperature.

On the compressively stressed side of the glass the cracks were parallel to the direction of applied compression. (This is perpendicular to the induced tensile stresses on that surface and corresponds to the tensile patterns observed on the opposite side except for the 90^{o} rotation.)

On both tensile and compressive surfaces, the parallel crack patterns, diviating regularly at "flaws" were observed, Figure 10.

Figure 10. "Compressive" Fracture Discontinuities

B. Pyrolytic Graphite

Many physical properties of pyrolytic graphite are already known, being found by experimental processes. It is known, also, that in any particular run in the production of pyrolytic graphite, the results may vary so much as to render the final product useless.[59, 60, 61, 62] It is the purpose of the studies presented here to explain the behavior of the graphite on a microstructural basis. Micro-studies were conducted to reveal the crystalline structure of pyrolytic graphite. An understanding of the crystalline structure of pyrolytic graphite will shed light on the mechanics of deposition, and furnish information to further understand the causes of fracture.

The very nature of pyrolytic graphite makes accurate microscopic observation difficult to obtain. Fresh, clean surfaces for examination are prepared by careful polishing, but with only a slight amount of pressure on the grinding wheel, the graphite becomes cold worked.

Various methods for dying and etching the surface to decorate the structure were tried, but with little success. Efforts were being directed to changing the surface composition of the pyrolytic graphite without changing the structure, and using dyes that react favorably with the new composition to view the structure of the graphite during the final month of the contract period.

Photomicrographs, taken with polarized light, have aided in the viewing of the structure. Magnification of 900 power and above have been especially revealing, but necessitate the tedious preparation of an almost perfectly polished specimen.

Pyrolytic graphite crystals, when viewed perpendicular to the c-axis, appears to form cone-like solids, characterized by parallel extinction with crossed nicols. Growth lines (for want of a better word) shown in Figures 11, 12, and 13, radiating outward from a central nucleation point are visible under polarized light. Laminations in the ab plain are clearly influenced by the boundaries of the structures. The laminations also have a central focal point which can be taken as the same point for the growth lines. When these structures are viewed paralled to the c-axis on a polished surface, nearly straight sided polygons are observed. Crystal boundaries are very distinct. Many of the polygons are six sides, although as many as twelve sides have been counted.

Figure 11. X60. View of crystal shape when viewed perpendicular to the c-axis. Bottom surface is the surface of nucleation. Taken with polarized light.

Figure 12. X60. Same orientation as Figure 11, but taken on a finely polished surface. The growth lines are clearly visible.

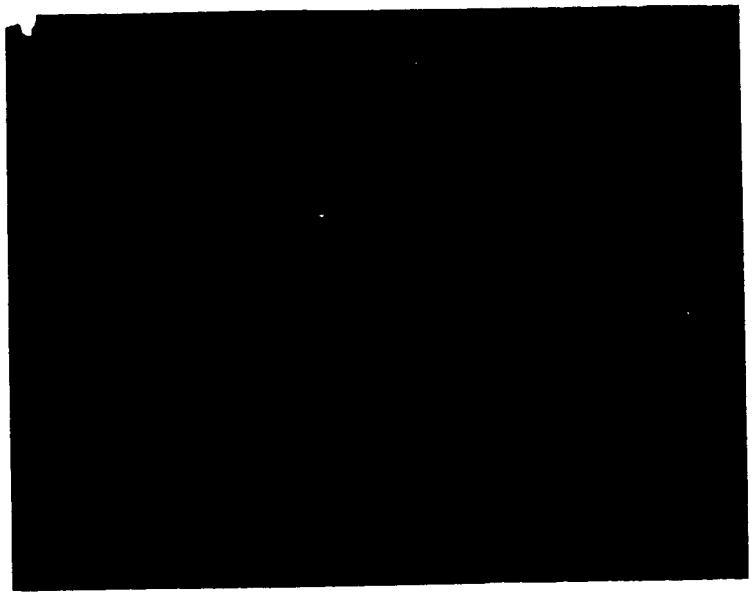

Figure 13. X900. Side view of the intersection between two crystals. The dark line is a delamination. The lighter vertical lines are growth lines.

In Figures 14 and 15, several of the polygons on the bottom surface (first nucleated) has concentric ring crack patterns. These cracks seem to be tensional, perhaps occurring during cooling after deposition. The center of these concentric fractures were not necessarily the center of the enclosing polygon. Dark spots, suggestive of nucleation points, were observed near the center of the bottom polygons of other samples of pyrolytic graphite. Although the surface was finely polished, there appeared to be an uneveness of the surface at the dark spot. Polygons of similar shape, but of larger size, were viewed on the top (last nucleated) surface of the specimens, shown in Figure 16. No dark spots or concentric fractures were observed.

Figure 14. X60. Polygons formed by crystal intersection. Bottom view or first nucleated surface. Concentric fracture rings are present.

Figure 15. X900. Area shown in rectangle in Figure 14.

Figure 16. X60. Polygons formed by crystal intersection. Top view or last nucleated surface. The photographed surface is flat and finely polished.

One side of the polygon, whether viewed on top or bottom, is always lighter than the other, providing good contrast for observation. The direction of polishing determines the light and dark sides of the polygon.

Based on the previous observations, it is concluded that the shape of these crystals are much like sections of a sphere. Deposition of pyrolytic graphite begins with a nucleation and grows outward in all directions until growth is interrupted by some object or another crystal.

The shape of the curves produced by the crystal boundaries when viewed perpendicular to the c-axis appears to be a catenary, represented in Figure 11. Therefore, any section of the crystal taken perpendicular to the ab plain and containing the c-axis will have what appears to be a catenary type outline. Although the outlines, when viewed perpendicular to the ab plain, vary with each crystal, the c-axis profile is very similar in any one sample of pyrolytic graphite.

A pyrolytic graphite sample was observed and then placed under a compressive force normal to the c-axis of about 200 pounds/in. The first sign of failure was delamination in the ab plain, perpendicular to the direction of the applied force. With increasing pressure, the specimen (1 X 1 X .5 cm) shattered into a fine angular powder. The fracture patterns, other than the delamination, could not be correlated with the crystalline structure of the pyrolytic graphite. This type of fracturing is indicative of internal stresses.

Delamination of pyrolytic graphite also occurs when a sample is subjected to nitric or sulfuric acid. A sample was allowed to stay in boiling sulfuric acid for five minutes.

When the sample was observed shortly after washing, it was noted that long chains of water and acid beads were being extruded from seemingly invisible laminations. This spontaneous extrusion continued for over four hours. The beads formed only on the sides of the samples that were perpendicular to the laminations.

VI. DISCUSSION OF RESULTS

In the etching studies it was surprising that so little correlation was found between the different decoration techniques. Levengood's water condensation technique was used to an advantage to "decorate" surface detail and the patterns which are formed seem extremely sensitive to surface treatments. Throughout this investigation, a "breath" pattern was used to distinguish between a cleaned or uncleaned slide, a diffusion-etched side, or the precise area which was etched and this could usually be determined from the pattern by the naked eye. Similarly,

under higher magnification, some of the detail remained in the water condensation pattern, but became less vivid as individual droplets were examined.

The NaF -HCl etch revealed minute surface defects invisible to the ordinary microscope. The patterns had fine detail and were observable under 100X or higher power. The "decoration" is said to consist of minute sodium silica flouride crystals deposited along the "flaw" sites.

Little depth is involved in the etching or decoration unless the etchant is allowed to remain in contact with the glass for an extended period of time. This technique is probably the best one for revealing minute surface damage and retaining a permanent record.

The diffusion of Li^+ ions into the glass to replace the Na^+ ions is the proposed mechanism for the alteration of the glass surface when the $LiNO_3$ -KNO_3 "etch" is used.[54] This explanation is plausible, however, the results indicate clearly that in the "etching", or diffusion process, the resulting altered surface glass is in tension during the "etching", and probably cracks in this process at the 200°C etching temperature rather than cracking upon cooling and from the induced differential contraction. This is partically confirmed by stressing the samples during the microscopic examination and observing the behavior of the cracks.

The crack pattern formed when a surface is stressed should be uniform if the etchant is uniform, and the surface is uniform. The $LiNO_3$ -KNO_3 mix was homogenized by melting and remaining molten overnight. The resulting mix was crushed as needed for the examination and is felt to be very uniform in composition. Assuming the etchant is uniform, the deviation in crack pattern can only be caused by a disturbance in the stress distribution since such complete orienting of the cracks (with applied stress) is observed. The resulting deviation in crack patterns are adaptable to stress analysis.

The deviations in crack behavior are apparently due to compositional inhomogenities extending at least a few microns into the surface. It would be interesting and informative to further section a sample, through a flaw, and etch the flaw in the depth plane also.

Little or no correlation has been observed between the NaF -HCl etch and the $LiNO_3$ -KNO_3 etch treatments. On a clean slide the NaF -HCl etch was tried and after etching, was examined. The same slide was diffused with $LiNO_3$ -KNO_3 in the same etched area and no correlation of the patterns was discernible. Both decorations, seemingly independent, could be simultaneously observed. The surface defects revealed by the NaF -HCl etch seemed to be just surface defects of minute depth, while the diffusion process neglects these defects of small depth and is influenced only by compositional inhomogenity or internal stresses induced by such inhomogenity, stone, etc.

The measurements of strength by loop stress technique has provided a simple tool with suffieient accuracy to reveal the sensitivity of glass fibers to surface conditions. While the data obtained are in reasonable agreement with other investigations,[55, 56, 57] the rather low initial strengths near zero time after forming are not in agreement with present concepts.

Stockdale[55] has shown that strength of glass may increase after immersion in water for some time or immediately after immersion in methy alcohol. These effects have been explained by proposing that the small organic molecules fill or surround the "flaw" reducing its effectiveness. Initial water immersion decreases strength while further exposure increases strength. This has been explained by the slight etching which first emphasized flaws and later etches them into a less effective state. Other postulations include capillary action initially building up pressure in fissures which reduce strength and later formation of gels which improve strength.

The sketchy results obtained on very fresh glass in this investigation indicated that the glass may be far from equilibrium in this early period and the absorption occurring at the surface on time dependent relaxation processes occurring in the glass may be extremely important in the ultimate brittle behavior.

Decoration by vapor condensation proved to be very sensitive, if carefully performed.

The dielectric measurements which relate the change in dielectric constant or permittivity to the applied pressure are not unique. Many investigators have measured, interferometrically, the change in index of refraction with pressure for many materials and since the two properties are related:

$$K = n^2$$

both properties measured at the same frequency, the change should be detachable. Standard capacitance measuring techniques are generally lacking in sensitivity, however, several methods are available to resolve 10^{-3} pfd. The bridge used had resolution to 2×10^{-3} pfd and it was reasoned would reveal any dielectric property changes since the resolution is about $\pm$ .01 per cent and the calculated change due to mechanical (elastic) deformation would amount to about 0.14 per cent at 60-70,000 psi.

In preliminary trials, deviations as well over one per cent were measured up to about 10,000 psi compression, however, the samples preparation and experimental difficulty encountered precluded the collection of accurate date as shown in Appendix III. As expected, when adequate precautions were taken to insure uniform loading, the results were much improved. The absence of deviation in dielectric constant when bending or torsion stresses are introduced was expected since the electrode

configuration "averages" the properties of the enclosed bar. For shear stresses, equal tension, and compression stresses, the effects cancel electrically and no deviation is detected. If, however, a material has compressive properties different from tensile properties (modulus, Poisson's Ratio) some deviations might ultimately be detected.

Since several per cent change in dielectric constant is achieved with 10,000 to 20,000 psi, the existing internal stresses in a material could easily introduce such areas of local disturbance that they could be detected by suitable electrical measurements. Unfortunately, local variations in density of the sample would probably yield the same effect as internal stress, but this must be investigated further.

It has become more apparent that many of the media which are normally assumed to be isotropic and uniform in properties can exhibit many forms of local inhomogenity - compositional, density, stress induced anisotropy. While these local disturbances are probably negligible in many ductile materials, their effects in brittle materials are of paramount importance and probably explain the wide deviations in measured property values for brittle materials.

Isotope decoration studies with P^{32} were concluded without demonstrating feasibility. While the isotope used showed no preferential absorption at the flaw sites, other isotopes may be more successful. With the sodium vapor decorations appearing so successful, an alkali metal isotope would be a good choice for future studies.

VII. RECOMMENDATIONS

Although the development and basic testing of the "brittle" class of materials is in the hands of the materials engineer, application is the responsibility of the structural designer, who in many cases has had little experience with these materials. If materials of this class are to be incorporated successfully as stress-bearing components, both technical groups must understand and appreciate these materials behavior.

Significant property evaluation should be made available to the designer, but data interpretation is needed as such property behavior differs from those of materials now in common use.

Further understanding of brittle fracture behavior of ceramic, cermet, and graphite materials is needed and should be gained through microstructure studies of polyscrystalline materials.

Particle size, orientation, stored strain energy, and dislocation effects on fracture behavior should be studied. Destructive as well as nondestructive approaches to material behavior should be further pursued.

VIII. CONCLUSIONS

Comprehensive nondestructive evaluation of ceramic, cermet, and graphite materials will only be developed as the result of extensive structural behavior studies. External as well as internal imperfection effects must be further understood in order to bring about fracture mechanism concepts which are applicable to design interpretation.

The influence of pressure on the measured dielectric constant of polycrystalline alumina was investigated and a 6 per cent change in permittivity was induced by 50,000 psi compression.

Glass and mica surfaces were investigated with "breath figures", and the techniques for producing these figures developed.

More information is needed before any final results can be obtained concerning the fracture mechanism of pyrolytic graphite. The catenary-aspect of the crystal shape is especially promising. By deriving the equation for the base shape of the c-axis profile of the crystals in any one sample of pyrolytic graphite, the surface tension between the crystals may be computed. This could lead to an index to classify pyrolytic graphite.

IX. REFERENCES

1. William H. Otto, "Relationship of Tensile Strength to Glass Fiber Diameter," J. Am. Ceram. Soc., 38, 122 (1955).

2. W. C. Levengood, "Study of Moisture-Condensation Patterns on Glass and Crystalline Surface," J. Am. Ceram. Soc., 38, 178 (1955).

3. Charles H. Greene, "Flaw Distribution and Variation of Glass Strength with Dimensions of the Sample," J. Am. Ceram. Soc., 39, 66 (1956).

4. V. K. Moorthy and F. V. Tooley, "Effect of Certain Organic Liquids on the Strength of Glass," J. Am. Ceram. Soc., 39, 215 (1956).

5. V. K. Moorthy, F. V. Tooley and C. F. Stockdale, "Influence of Water Immersion Treatment on Tensile Strength of Glass: Effect of Temperature," J. Am. Ceram. Soc., 39, 395 (1956).

6. Ivan B. Cutler, "Strength Properties of Sintered Alumina in Relation to Porosity and Grain Size," J. Am. Ceram. Soc., 40, 20 (1957).

7. E. D. Lynch and F. V. Tooley, "Effect of Stress and Temperature During Forming on Strength of Glass," J. Am. Ceram. Soc., 40, 107 (1957).

8. Laszlo Mattyasovszky - Zsolnay, "Mechanical Strength of Porcelain," J. Am. Ceram. Soc., 40, 299 (1957).

9. A. E. Gorum, F. R. Parker and J. A. Pask, "Effect of Surface Conditions on Room Temperature Ductility of Ionic Crystals," J. Am. Ceram. Soc., 41, 161 (1958).

10. J. H. Westbrook, "Temperature Dependence of Strength and Brittleness of Some Quartz Structures," J. Am. Ceram. Soc., 41, 433 (1958).

11. F. P. Knudsen, "Dependence of Mechanical Strength of Brittle Polycrystalline Specimens on Porosity and Grain Size," J. Am. Ceram. Soc., 42, 376 (1959).

12. J. B. Wachtman, Jr. and L. H. Maxwell, "Strength of Snythetic Single Crystal Sapphire and Ruby as a Function of Temperature and Orientation," J. Am. Ceram. Soc., 42, 432 (1959).

13. George R. Pulliam, "Precipitation in Microscopic Cracks," J. Am. Ceram. Soc., 42, 477 (1959).

14. R. E. Mould and R. D. Southwick, "Strength and Static Fatigue of Abraded Glass under Controlled Ambient Conditions: I, General Concepts and Apparatus," J. Am. Ceram. Soc., 42, 542 (1959).

15. R. E. Mould and R. D. Southwick, "Strength and Static Fatigue of Abraded Glass Under Controlled Ambient Conditions: II, Effect of Various Abrasions and the Universal Fatigue Curve," J. Am. Ceram. Soc., 42, 582 (1959).

16. R. E. Mould, "Strength and Static Fatigue of Abraded Glass under Controlled Ambient Conditions: III, Aging of Fresh Abrasions, "J. Am. Ceram. Soc., 43, 160 (1960).

17. E. E. Shand, "Stress Behavior of Brittle Materials," J. Am. Ceram. Soc., 38, 653 (1959).

18. A. A. Griffith, 'Phenomenaof Rupture and Flow in Solids," Trans. Roy. Soc. (London) A 221, 163-98 (1921).

19. W. C. Levengood and W. E. Fowler, "Morphology of Fractures in Polished Glass Surfaces," J. Am. Ceram. Soc., 40, 31 (1957).

20. N. V. Glike, "Use of 'Dew' Method for Investigating Spiral Growth Steps," Doklady Akad, Nauk S.S.S.R. 90 541 (1953).

21. J. E. May and M. L. Kronberg, "Temperature Dependence of Plastic Yield Stress of Single Crystals of Magnesium Oxide, "J. Am. Ceram. Soc., 43 525 (1960).

22. M. L. Kronberg and J. E. May, "Ductility of Magnesium Oxide Single Crystals," J. Am. Ceram. Soc., 43, 438 (1960).

23. A. E. Gorum, W. J. Luhman and J. A. Pask, "Effect of Impurities and Heat Treatment on Ductility of MgO," J. Am. Ceram. Soc., 43, 241 (1960).

24. N. K. Adam, The Physics and Chemistry of Surfaces, 3rd Ed., Oxford University Press, (1949).

25. H. E. Simpson, "Adaptation of Replica Technique to Measurement of Surface Durability of Glass," J. Am. Ceram. Soc., 38, 81 (1955).

26a. H. M. Parikk, "Effect of Atmosphere on Surface Tension of Glass," J. Am. Ceram. Soc., 41, 18 (1958).

26b. A. F. Van Zee and H. M. Noritake, "Measurements of Stress-Optical Coefficient and Rate of Stress Release in Commercial Soda-Lime Glasses," J. Am. Ceram. Soc. 41, 164, (1958).

27. Martin Goddstein and T. H. Davies, "Glass Fibers with Oriented Chain Molecules," J. Am. Ceram. Soc., 38, 223 (1955).

28. W. D. Kingery, "Note on Thermal Expansion and Microstresses in Two-Phase Compositions," J. Am. Ceram. Soc., 40, 351 (1957).

29. E. A. Bush and F. A. Hummel, "High-temperature Mechanical Properties of Ceramic Materials: I, Magnesium Dititanate," J. Am. Ceram. Soc., 41, 189 (1958).

30. E. A. Bush and F. A. Hummel, "High-temperature Mechanical Properties of Ceramic Materials: II Beta Eucyptite," J. Am. Ceram. Soc., 42, 388 (1959).

31. Richard M. Fulrath, "Internal Stresses in Model Ceramic Systems," J. Am. Ceram. Soc., 42, 423 (1959).

32. J. B. Wachtman, Jr. and D. G. Lam, Jr., "Young's Modulus of Various Refractory Materials as a Function of Temperature," J. Am. Ceram. Soc., 42, 254 (1959).

33. A. S. Argon, Y. Hori and E. Growan, "Indention Strength of Glass," J. Am. Ceram. Soc., 43, 86 (1960).

34. L. Ainsworth, "Diamond Pyramid Hardness of Glass in Relation to Strength and Structure of Glass: I - Investigation of the Diamond Pyramid Hardness Test Applied to Glass," J. Soc. Glass Technol. 38 (184) 479T (1954); "II-Silicate Glasses" Ibid 38, (185), 401T, (1954); "III -Structure of Borosilicate Glasses, "Ibid 536T.

35. Paul Grodzinski, "Microhardness of Flat Glass and Tempered Glass," Glastech, Ber. 26, 309, (1953), Ceramic Abstracts 1956, (2), 32g.

36. O. L. Anderson and H. E. Bommel, "Ultrasonic Absorption in Fused Silica at Low Temperatures and High Frequencies," J. Am. Ceram. Soc., 38, 125 (1955).

37. Maurice L. Huggins, "The Structure of Glass," J. Am. Ceram. Soc., 38, 172 (1955).

38. S. L. Blum, "Some Physical Factors Affecting the Internal Damping of Glass," J. Am. Ceram. Soc., 38, 205 (1955).

39. B. L. Steierman, J. C. C. Wu, and J. M. McCormick, "Note on Ultrasonic Absorption of Glass at Elevated Temperatures," J. Am. Ceram. Soc., 38, 211 (1955).

40. D. T. Livey and P. Murray, "Surface Energies of Solid Oxides and Carbides," J. Am. Ceram. Soc., 39, 363 (1956).

41. A. Winter, "Glass Formation," J. Am. Ceram. Soc., 40, 54 (1957).

42. J. E. Burke, "Role of Grain Boundaries in Sintering, "J. Am. Ceram Soc., 40, 80 (1957).

43. Ivan B. Cutler er al, "Sintering of Alumina at Temperatures of 1400°C. and Below," J. Am. Ceram. Soc., 40, 134 (1957).

44. J. B. Wachtman and L. H. Maxwell, "Plastic Deformation of Ceramic-Oxide Single Crystals, II," J. Am. Ceram. Soc., 40, 377 (1957).

45. W. D. Kingery, "Surface Tension of Some Liquid Oxides and their Temperature Coefficients," J. Am. Ceram. Soc., 42, 6 (1959).

46. E. B. Shand, "Breaking Stress of Glass Determined from Dimensions of Fracture Mirrors," J. Am. Ceram. Soc., 42. 474 (1959).

47. H. Conrad and H. L. Sujata, "Dislocation Theory Applied to Structural Design Problems in Ceramics," Materials Advisory Board Symposium on Design with Brittle Materials paper, Washington, D. C., 1960.

48. J. C. Bowman, R. M. Bushong, "Graphite and Refractory Borides on High Temperature Structural Materials," Ibid.

49. V. Weiss, J. G. Sesler, and G. Sachs, "Analysis of Brittle Fracture in Sheet Materials," Ibid.

50. R. D. Chipman, "The Role of Bending Data in Design with Brittle Materials," Ibid.

51. W. H. Duckworth and A. Rudnick, "Some Engineering Aspects of the Strength of Ceramic Materials," Ibid.

52a. W. C. Levengood, "Study of Moisture Condensation Patterns on Glass and Crystalline Surfaces," J. Am. Ceram. Soc. 38, 178, (1955).

52b. W. C. Levengood, "Effect of Origin Flaw Characteristics on Glass Strength," J. Appl. Phys. 89 820 (1958).

52c. W. C. Levengood, and T. S. Vong, "Dislocation Type Defects in Glass," J. Chem. Phy. 31 1104 (1959).

53. J. E. Gordan, D. M. Marsh and Margaret E. Parratt, "On the Strength and Structure of Glass," Proc. Ray Soc. (London) A 249 (1959).

54a. F. M. Ernsberger, "Detection of Strength-Imparing Surface Flaws in Glass," Proc. Roy. Soc. A257, 1289, 213 (1960).

54b. W. C. Levengood and T. S. Vong, "Observations concerning Delayed Elastic Effects in Glass," J. Opt. Soc. Am. 49 61 (1959).

54c. R. J. Charles, "Static Fatigue of Glass I, "J. Appl. Phys. 29 1549 (1958).

55. G. F. Stockdale, F. V. Tooley and C. W. Ying, "Changes in the Tensile Strength of Glass caused by Water Immersion Treatment," J. Am. Ceram. Soc. 34 116 (1951).

56. W. H. Otto, "Relationship of Tensile Strength of Glass Fibers to Diameter," J. Am. Cer. Soc., 38, 122, (1955).

57. E. D. Lynch and F. V. Tooley, "Effect of Stress and Temperature during Forming on the Strength of Glass," J. Am. Ceram. Soc., 40, 107, (1957).

58. J. E. Gordon, D. M. Marsh and Margaret E. Parratt, "On the Strength and Structure of Glass," Proc. Ray Soc. (London), A, 249 (1959).

59. J. J. Cacciotti, Graphite and its Properties, Flight Propulsion Laboratory Department, General Electric Company, June, 1960.

60. Farie, F. E., Green, L., Jr., Smith, C. A., "The Thermal Dependence of the Elastic Moduli of Polycrystalline Graphite " J. Appl. Phy. 23 pp. 89-95, (1952).

61. Mrozowski, S., "Anisotropy of Thermal Expansion and Internal Stresses in Polycrystalline Graphite and Carbons," Bull. Am. Phy. Soc. 27, pp. 47, (1952).

62. _____, "Electrical Resistivity of Polycrystalline Graphite and Carbons," Physical Review, 77, pp 838, (1950).

APPENDIX I

MAXIMUM STRESS IN AN ELASTIC LOOP

Problem: Find the maximum outer fiber stress in a loop of glass fiber by considering only the geometry of the loop and fiber diameter. The principal parameters which should be considered are the angle at which the ends cross and some size parameter for the loop.

If the radius of curvature of the loop can be found at any point, and the point of minimum radius is selected, the maximum stress can be found from the approximate relation.

$$S_{max} = \frac{E R_{fiber}}{R_{curv}}$$

S_{max} = Maximum stress in outer fiber
E = Modulus of Elasticity
R_{fiber} = Maximum radius to outer point of Sections
R_{curv} = Minimum radius of curvature

Generalizing, the problem is closely related to the classic "elastica" problem where a thin column or wire is compressed at each end, the force being applied at "pinned" joints free to move in the "X" direction as the force is increased. (Fig.17) The solution to this problem is usually for the force required to buckle the column and, since most materials yield before failure, the "maximum outer fiber stress" would only be applicable up to the yield point. When the yield point is exceeded the geometry of the loop changes, and the equations which describe the "elastica" problem are no longer applicable.

First, solving the classic "elastica" problem; let the thin elastic rod be placed on the "X" axis and compressive force applied along the "X" axis as in Fig. 17.

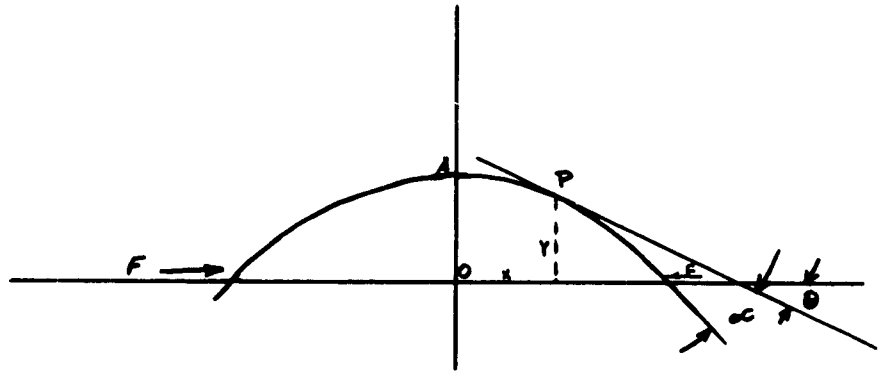

Figure 17. Elastica Geometry

The forces F are equal and opposite; the angle α is the angle which the end of the rod makes with the "X" axis. The bending moment equation at any point then is:

$$\frac{EI}{R} = M = -Fy \tag{1}$$

Where E = Modulus of Elasticity
I = Moment of inertia of the cross section
R = Radius of curvature
M= bending moment

If S is the arc length AP, we have

$$\frac{I}{R} = \frac{d\theta}{dS} = \frac{-dy}{dS}\frac{d\theta}{dy} = \sin\theta \frac{d\theta}{dy} \tag{2}$$

and (1) may be written

$$EI \sin\theta \, d\theta = -Fy \, dy \tag{3}$$

For ease of manipulation let $C^2 = \frac{EI}{F}$

Then intergration of (3) yields

$$\frac{Y^2}{2} = C^2 \cos\theta + C_1 \tag{4}$$

To solve for C_1 the constant of integration, apply the boundary conditions at Y = O where $\alpha = \theta$. Thus $C_1 = -C^2 \cos\alpha$ and (4) becomes

$$Y^2 = 2C^2(\cos\theta - \cos\alpha)$$

$$Y = \sqrt{2}\, C \sqrt{\cos\theta - \cos\alpha} \tag{5}$$

substitution $\cos\theta = 1 - 2\sin^2\frac{\theta}{2}$; $\cos\alpha = 1 - 2\sin^2\frac{\alpha}{2}$

$$Y = \sqrt{2}\, C \sqrt{1 - 2\sin^2\frac{\theta}{2} - 1 + 2\sin^2\frac{\alpha}{2}}$$

$$Y = \sqrt{2}\, C \sqrt{2\left(\sin^2\frac{\alpha}{2} - \sin^2\frac{\theta}{2}\right)}$$

$$Y = 2C \sqrt{\sin^2\frac{\alpha}{2} - \sin^2\frac{\theta}{2}} \tag{6}$$

$\sin\frac{\alpha}{2}$ is a constant for any given F value so let $K = \sin\frac{\alpha}{2}$. Also substitute $\sin\frac{\theta}{2} = K \sin\phi$ in (6).

$$Y = 2C\sqrt{K^2 - K^2 \sin^2 \phi}$$

$$Y = 2CK \cos \phi \tag{7a}$$

or

$$Y = 2\frac{EI}{F} \sin\frac{\alpha}{2} \cos \phi \tag{7b}$$

where $$\phi = \sin^{-1}\left(\frac{\sin\frac{\theta}{2}}{\sin\frac{\alpha}{2}}\right)$$

To solve for the length of the curve and X parametrically, the integration of ds is necessary. From (3) replacing $\sin\theta$ by $\frac{dy}{ds}$

$$EI\frac{dy}{ds} = -Fy\frac{dy}{d\theta}$$

$$ds = C^2\frac{d\theta}{Y} \tag{8}$$

substituting (7a) for Y

$$ds = \frac{C\, d\theta}{2K\cos\phi} \tag{9}$$

Since $K \sin\phi = \sin\frac{\theta}{2}$ differentiating, we have

$$K\cos\phi\, d\phi = \cos\frac{\theta}{2}\frac{d\theta}{2}$$

$$d\theta = \frac{2K\cos\phi\, d\phi}{\cos\frac{\theta}{2}}$$

$$d\theta = \frac{2K\cos\phi\, d\phi}{\sqrt{1 - K^2\sin^2\phi}} \tag{10}$$

Combining (9) and (10)

$$ds = \frac{d\phi}{\sqrt{1 - K^2\sin^2\phi}}$$

$$ds = \frac{C\, d\phi}{\sqrt{1 - K^2\sin^2\phi}}$$

$$S = C\int \frac{d\phi}{\sqrt{1 - K^2\sin^2\phi}} \tag{11}$$

To establish limits; when $\phi = 0^o$, X = 9 and y is a maximum, thus integrating from 0 to ϕ gives the length of the curve from (0, Y) to P (X, Y). Or integrating from 0 to $\frac{\pi}{2}$ gives the length of one-half the curve, since at $\frac{\pi}{2}$ $\text{Sin}\,\phi = 1 = \frac{\text{Sin}\frac{\phi}{2}}{\text{Sin}\frac{\alpha}{2}}$ and thus $\frac{\theta}{2} = \frac{\alpha}{2}$ and this only occurs at Y = O

so equation (10) becomes for the total length of the curve

$$S = 2C \int_0^{\frac{\pi}{2}} \frac{d\theta}{\sqrt{1 - K^2 \text{Sin}^2 \theta}} \tag{11a}$$

or for the length of the curve around a loop, integrate to the value of ϕ corresponding to the point (0, Y)

$$= 2C \int_0^{\phi} \frac{d\phi}{\sqrt{1 - K^2 \text{Sin}^2 \phi}} \tag{12}$$

This integral is the form of an elliptic integral of the first kind usually denoted by the symbol $F(K, \phi)$; if K and ϕ are known, $F(K, \phi)$ may be obtained from a table.

$$S = 2C\, F(K, \phi) \tag{13}$$

To find X, in terms of ϕ, we have

$$dX = \text{Cos}\,\theta\, ds$$

$$dX = (1 - 2K^2 \text{Sin}^2 \phi) \frac{C\, d\phi}{\sqrt{1 - K^2 \text{Sin}^2 \phi}}$$

$$dX = 2C \frac{(1 - K^2 \text{Sin}^2 \phi) - 1}{\sqrt{1 - K^2 \text{Sin}^2 \phi}}\, d\phi$$

$$dX = C \left[2\sqrt{1 - K^2 \text{Sin}^2 \phi} - \frac{1}{\sqrt{1 - K^2 \text{Sin}^2 \phi}} \right] d\phi$$

$$X = 2C \int_0^{\phi} \sqrt{1 - K^2 \text{Sin}^2 \phi}\, d\phi - C \int_0^{\phi} \frac{d\phi}{1 - K^2 \text{Sin}^2 \phi}$$

Or $$X = C \left[2E(K, \phi) - F(K, \phi) \right] \tag{14}$$

Where $E(K, \phi)$ is an elliptic integral of the second kind and $F(K, \phi)$ is an elliptic integral of first kind

or substituting (13) in (14)

$$X = 2C\ E(K, \phi) - \frac{S}{2} \tag{15}$$

The three equations which describe parametrically, the curve formed by a thin rod compressed as in Fig. 17 are thus

$$Y = 2CK \cos \phi \tag{7a}$$

$$X = C\left[2\ E(K, \phi) - F(K, \phi)\right] \tag{14}$$

$$S = 2CF(K, \phi) \tag{13}$$

where:

$$K = \sin\frac{\alpha}{2} \qquad C = \sqrt{\frac{EI}{F}}$$

$$\phi = \sin^{-1} \frac{\sin\frac{\theta}{2}}{\sin\frac{\alpha}{2}}$$

By inspection, it can be seen that these general equations are also applicable to figure 18a and 18b, since the loading geometry, notation, and bending moment equations are the same.

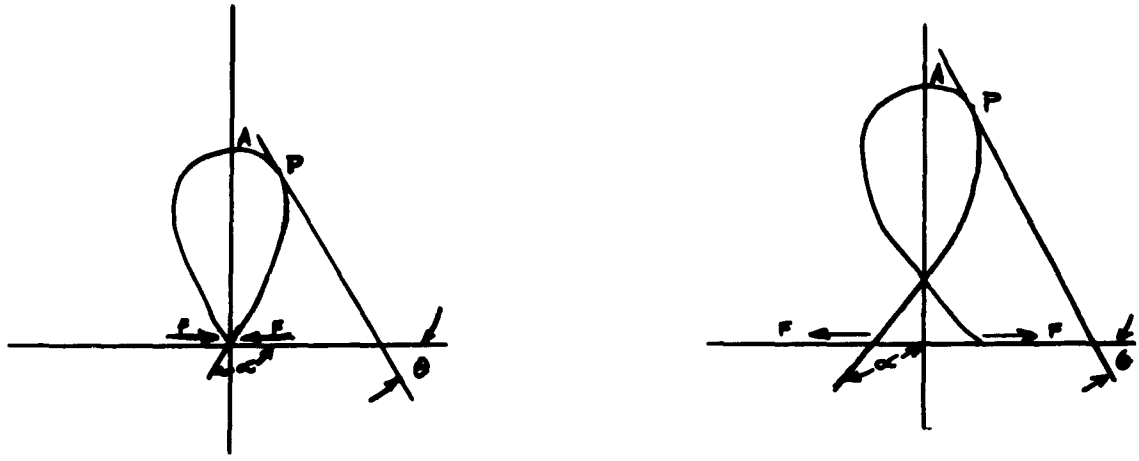

(a) (b)

Figure 18. The Loading Geometry of Fiber Loops.

Thus far, only the classical "elastica" problem has been repeated. For closed loops, a point (0, Y) must exist, and Figure 18 a is the limiting case where the ends meet at (0, 0); solving for the parameters which describe this geometry:

$$X = 0,\ Y = 0\ \alpha = \theta\ \ \phi = 90^\circ$$

$$X = 0 = C\left[2E(K,\phi) - F(K,\phi)\right]$$

therefore

$$2E(K,\phi) = F(K,\phi)$$

$$\phi = 90^\circ,\ 2E(K,90^\circ) = F(K,90^\circ)$$

interpolating from tables $K = \text{Sin } 65^\circ 21' = \text{Sin } \frac{\alpha}{2}$

$$F(K,90^\circ) = 2.3212$$

Therefore, $\frac{\alpha}{2} = 65^\circ 21'$ ($\alpha = 130^\circ 42'$) the angle between the ends of the loop is $\left[180^\circ - 2(180^\circ - 130^\circ 42')\right] = 2(130^\circ 42') - 180^\circ = 81^\circ 24'$

the length of the loop is:

$$\ell = S = 2C(2.3212)$$

$$\ell = S = 4.6414C$$

and Y_{max} or height of the loop is:

$\phi = 0$ because $\theta = 0$ at Y_{max} and $\text{Sin } \phi = \dfrac{\text{Sin } \frac{\theta}{2}}{\text{Sin } \frac{\alpha}{2}}$

$\therefore$ $\text{Cos } 0^\circ = 1$

$$Y = 2CK$$

$$Y = 2C \text{ Sin } 65^\circ 21'$$

$$Y = (1.81726)C$$

or $$\frac{Y}{\ell} = \frac{1.81726\cancel{\ell}}{4.6414\cancel{\ell}} = .392$$

For this geometry,

$$\frac{EI}{R} = -Fy \tag{1}$$

solving for R

$$R = -\frac{EI}{FY} = -\frac{C^2}{Y} \tag{15}$$

substitution (7a) for Y

$$R = - \frac{C}{2K \cos \phi} \tag{16}$$

but since we are not concerned with the force required to form a loop, and C is a function of the force solve (13) for C and substitute in (16).

$$R = \frac{\ell}{4(K)(\cos \phi)[F(K, \phi)]} \tag{17}$$

Since the maximum stress occurs at $Y_{max,}$ ($\cos \phi = 1$) then for maximum stress (minimum radius of curvature)

$$R_{min} = \frac{\ell}{4K[F(K, \phi)]} \tag{18}$$

where ℓ is equal to S for K = Sin 65°21' but will be defined more generally later.

Expression (18) is applicable to a loop geometry which can be generated in the matter described in the development where the angle between the ends of the fibers is maintained at 81°24' (at the intersection).

Since any fixture which applies a load to decrease the size of the loop may cause deviations from this angle, it is instructive to calculate the error involved should the above geometry not be observed, or to derive a suitable expression for calculating the radius of curvature for outer loop geomerties.

Consider any loop; the intersection of the loop ends occurs at X = 0 thus for any loop

$$2E(K, \phi) = F(K, \phi)$$

and these values can be derived from tables and plotted K vs ϕ to give the locus of K and ϕ values between K = Sin. 65°20' and K = Sin 90° which satisfy the conditions for forming a loop. A list of such values has been prepared in Table I.

TABLE I

List of some Values for $\frac{\alpha}{2}$, ($\mathrm{Sin}^{-1}K$), and ϕ which satisfy the condition $X = 0$

ϕ	$K = \mathrm{Sin}\frac{\alpha}{2}$ $\frac{\alpha}{2}$	$F(K, \phi)$	$\mathrm{Sin}\ \phi$	$\frac{K}{\mathrm{Sin}\frac{\alpha}{2}}$	$\mathrm{Sin}\frac{\theta}{2}$	$\frac{\theta}{2}$
90°	65°21'	2.3212	1.000	.90887	.90887	65°21'
89°	65°50'	2.2983	.99985	.91236	.91222	65°49'
88°	66°29'	2.2787	.99939	.91694	.91638	66°24'
87°	66°58'	2.2599	.99863	.92028	.91902	66°47'
86°	67°47'	2.2367	.99756	.92576	.92350	67°27'
85°	68°19'	2.2224	.99619	.92924	.92570	67°46'
84°	69°21'	2.1978	.99452	.93431	.92919	68°18'
83°	69°57'	2.1825	.99255	.93939	.93239	68°49'
82°	70°49'	2.1292	.99027	.94447	.93528	69°16'
81°	71°46'	2.1052	.98769	.94979	.93810	69°44'
80°	72°48'	2.0804	.98481	.95528	.94077	70°11'
79°	74° 2'	2.0563	.98163	.96142	.94376	70°82'
78°	75°21'	2.0313	.97815	.96749	.94635	71° 2'
77°	76°56'	2.0076	.97437	.97411	.94914	71°47'
76°	78°45'	1.9832	.97030	.98079	.95166	72° 7'
75°	80°56'	1.9583	.96593	.98751	.95387	72°32'
74°	84° 8'	1.9343	.96126	.99476	.95622	72°59'
73°18'	90°	1.9121	.95782	1.0000	.95782	73°18'

$$\mathrm{Sin}\ \phi = \frac{\mathrm{Sin}\frac{\theta}{2}}{\mathrm{Sin}\frac{\alpha}{2}}$$

$$\mathrm{Sin}\frac{\theta}{2} = \mathrm{Sin}\ \phi\ \mathrm{Sin}\frac{\alpha}{2}$$

In Table I the values of $F(K, \phi)$ correspond to the values of ϕ, $\frac{\alpha}{2}$ and $\frac{\theta}{2}$ for X = 0, the "end" of the loop. Values for $\frac{\theta}{2}$ have been calculated which represent the tangent to the curve at X = 0. Calculating the angle between the ends of the loop β, corresponding to $\frac{\theta}{2}$ values in informative; these values are found in Table II.

In equation (18) ℓ was defined as the loop length when $\frac{\alpha}{2} = 65^{\circ}21'$. If, however, the length of a loop is maintained constant and only the angle of intersection is changed, this is equivalent to varying C and $F(K, \phi)$ to maintain ℓ constant. Where $F(K, \phi)$ represents the values found in Table I for X = 0.

$$\ell = 2\ CF(K, \phi)$$

where K, ϕ represent values for X = 0

Then (18) becomes:

$$R = \frac{\ell_{\text{loop}}}{4K\ F(K, \phi)} \tag{18}$$

Where K and values for $F(K, \phi)$ correspond to these at X = 0; these can be found for any angle of intersection by referring to Table I.

If we consider a fixture which holds an elastic rod in a loop, and which by decreasing the loop length applies an increasing load, the magnitude of errors due to slight misalignment must be calculated. Referring to (18), and selecting 90° as the desired angle of intersection, β, the quantity $4\ KF(K, \phi)$ becomes a constant, 8.246 and (18) may be rewritten.

$$R_{min} = \frac{\ell_{\text{loop}}}{8.246} \tag{19}$$

If the angle of intersection, β, changes, the quantity $KF(K, \phi)$ changes slightly and this has been tabulated in Table II. By rationalizing values in terms of the value for 90° the fractional error can be calculated (Table II) and these values have been plotted as percentage in Fig. 19.

It can be seen that for the range of values of possible with the loop geometry described, the error is always less than about 7 per cent; for typical misalignments of $\pm 5^{\circ}$ the error is less than ± 2 per cent.

If certain restraint and bending moments are applied by the clamping of the ends, it is possible to obtain intersection angles less than $\frac{\alpha}{2} = 65^{\circ}21'$. To explore the effect of such a condition a single trial calculation has been made revising the original geometry slightly.

TABLE II

List of some Values for $\frac{\theta}{2}$ and β which

satisfy the condition X - O

$\frac{\theta}{2}$	β	K F(K, ϕ)	Fract error
60°	60°*	*	1.115
65°21'	81°24'	2.1097	1.0234
65°49'	83°16	2.0969	1.0172
66°24'	85°36'	2.0894	1.0136
66°47'	87°8'	2.0715	1.0048
67°27'	89°48'	2.0614	1.0000
67°46'	91°04'	2.0466	.9927
68°18'	93°12'	2.0347	.9870
68°49'	95°16'	2.0220	.9809
69°16'	97°4'	2.0110	.9756
69°44'	98°56'	1.9995	.9700
70°11'	100°44'	1.9874	.9641
70°42'	102°48'	1.9770	.9591
71°02'	104°8'	1.9653	.9534
71°17'	107°8'	1.9556	.9487
72°7'	108°28'	1.9451	.9436
72°32'	110°8'	1.9338	.9381
72°59'	110°56'	1.9239	.9333
73°18'	113°12'	1.9191	.9310

*See explanation following Fig. 20 regarding calculation or error

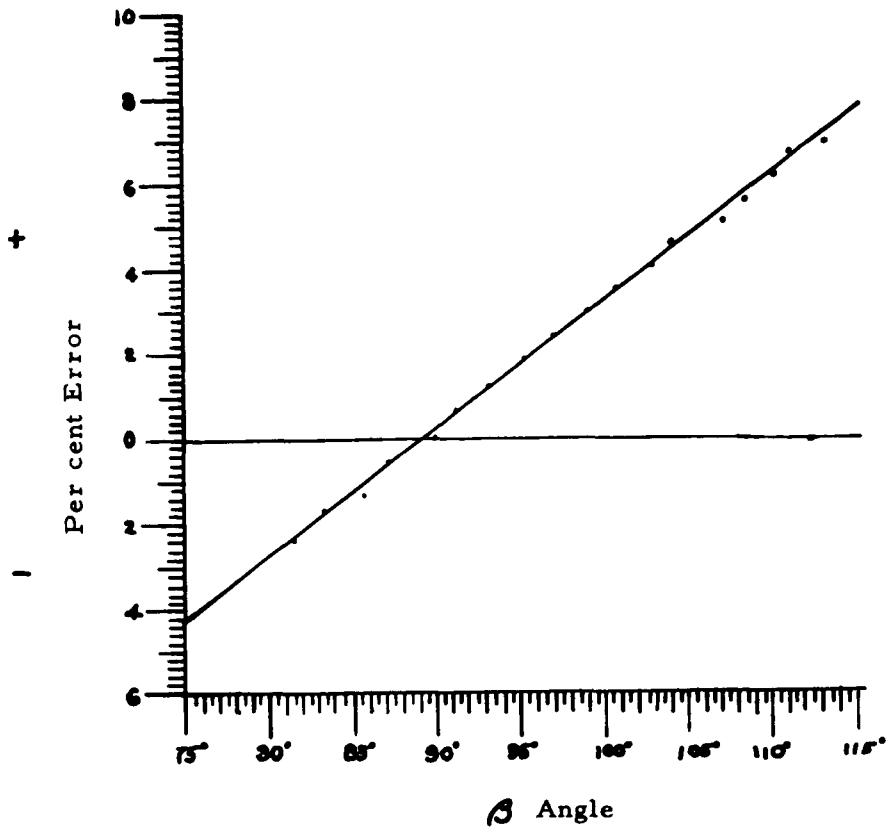

Figure 19. Per cent error in stress measurements introduced by variation in actual β angle from 90°.

If a long thin rod with pin joints not at the ends is subjected to loading as in Fig. 20 then the basic equations of the elastica still apply, but the length of the loop must be calculated as follows:

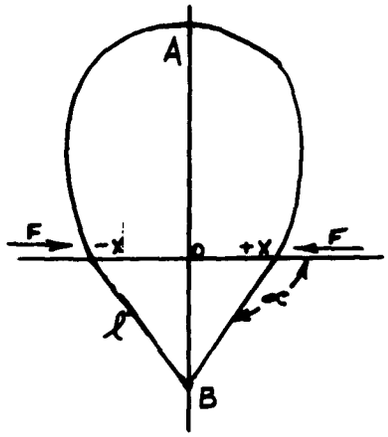

XB and -XB are straight line extensions of the curve.

Fig. 20

$$\ell_{loop} = 2\,CF(K, 90^\circ) + 2\ell'$$

$$\frac{X}{\ell'} = \cos\alpha \qquad \ell' = \frac{X}{\cos\alpha}$$

$$\text{but } X = C\left[2E(K, 90^\circ) - F(K, 90^\circ)\right]$$

$$\ell' = \frac{X}{\cos\alpha} = \frac{C\left[2.4222 - 2.1565\right]}{.5}$$

for $\frac{\alpha}{2} = 60^\circ$

$\alpha = 120^\circ$

$180^\circ - \alpha = 60^\circ$

$2\ell' = C[1.062]$

$F(60^\circ, 90^\circ) = 2.1565$

$2E(60^\circ, 90^\circ) = 2.4222$

$\cos\alpha = \cos(180^\circ - \alpha) = \cos 60^\circ = .5$

$\sin\frac{\alpha}{2} = \sin 60^\circ = .866$

$$\ell_{loop} = C\left[(4.313) + 1.062\right]$$

$$\ell_{loop} = C\left[5.375\right]$$

for $\frac{\alpha}{2} = 60^\circ$ the length S from -X to +X is:

$$S = 2C\,F(60^\circ, 90^\circ)$$

$$S = 4.313C$$

The exact expression for R at $\frac{\alpha}{2} = 60^\circ$ is:

$$R_{min} = \frac{S}{4\,K\,F}(60^\circ, 90^\circ) = \frac{4.313C}{2\,(4)\,(.866)(2.1565)}$$

$$R_{min} = \frac{C}{1.732} \qquad \text{(actual)}$$

If calculated <u>assuming</u> the intersection were 90° rather than the actual 60° but maintaining the loop length constant: from (19)

$$R_{min} = \frac{C\ 5.375}{8:246} \qquad \text{(assumed)}$$

$$R_{calc} = \frac{C}{1.54} \qquad \text{(assumed)}$$

Rationalizing:

$$\frac{R_{cal}}{R_{act}} = 1,1117$$

or the error of such a false assumption is about 12 per cent.

Since this calculation represents a 30° error in the assumed angle of intersection, it is conservative to say that the error due to misalignment or inaccurate measurement of the angle or intersection will always be less than $\pm$ 1/2 per cent per degree deviation from perpendicular intersection. In practice the angular error can be easily maintained less than $\pm$ 3° and the error from this source will be less than $\pm$ 2 per cent. This is negligible, since the error in measuring the diameter of the fibers, the uniformity of the diameter, and the ellipsiticy of the fiber will introduce larger errors in the final calculations.

APPENDIX II

NOMOGRAM FOR CALCULATION OF MAXIMUM STRESS IN AN ELASTIC LOOP

Figure 21. NOMOGRAM FOR CALCULATION OF MAXIMUM STRESS IN A UNIFORM, ELASTIC LOOP

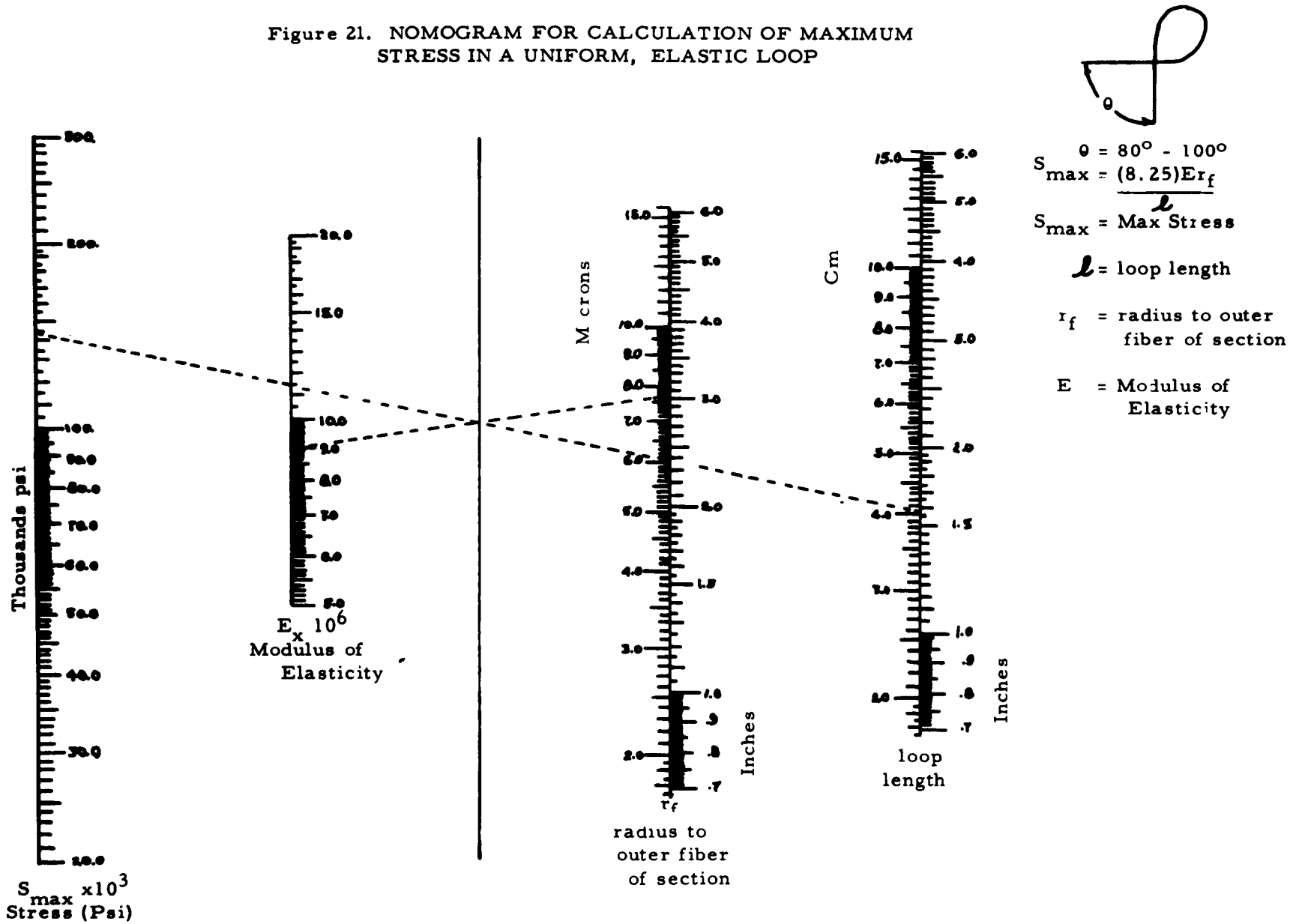

APPENDIX III

DIELECTRIC RESIDUAL STRESS ANALYSIS

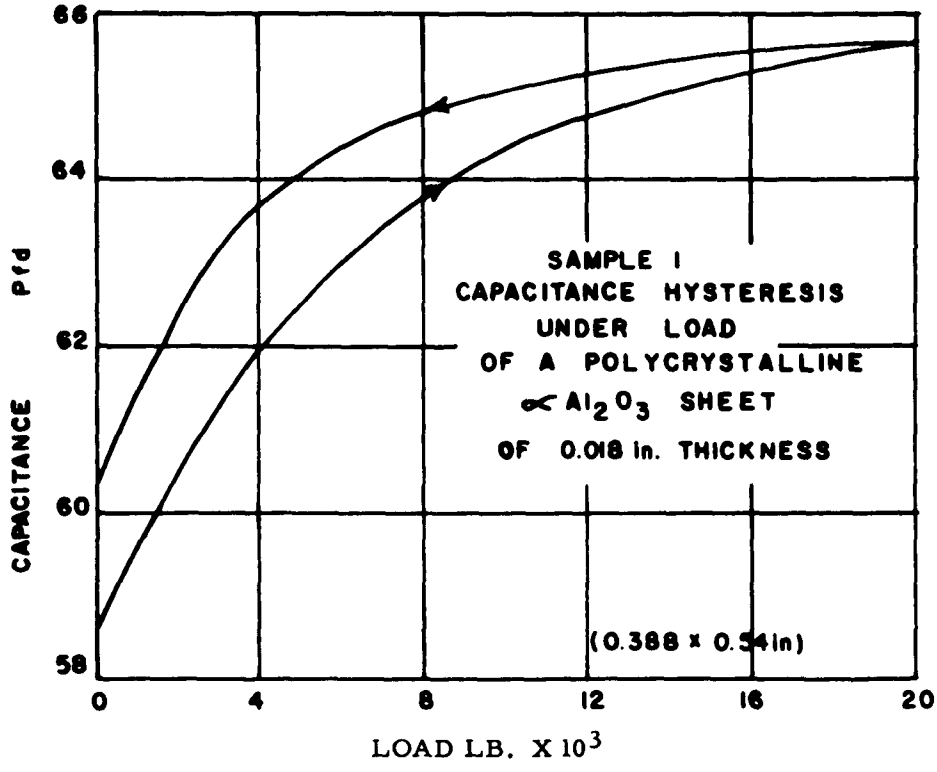

Figure 22. Capacitance Hysteresis Under Load

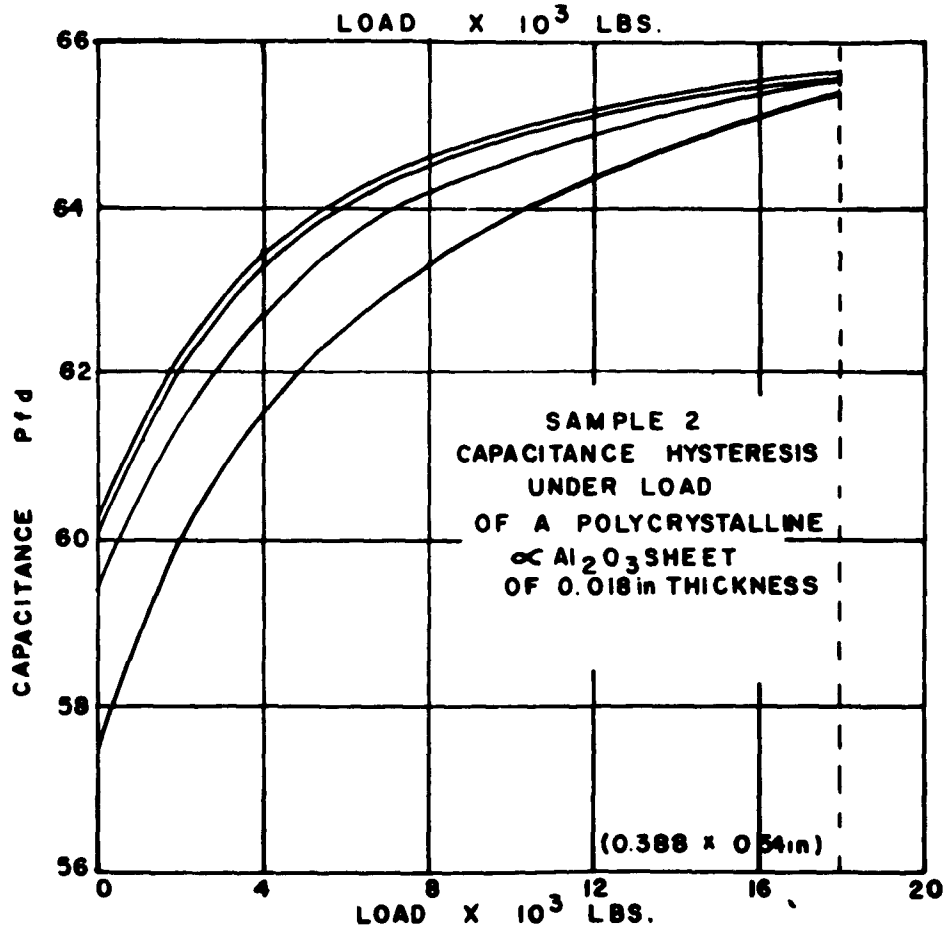

Figure 23. Capacitance Hysteresis Under Load

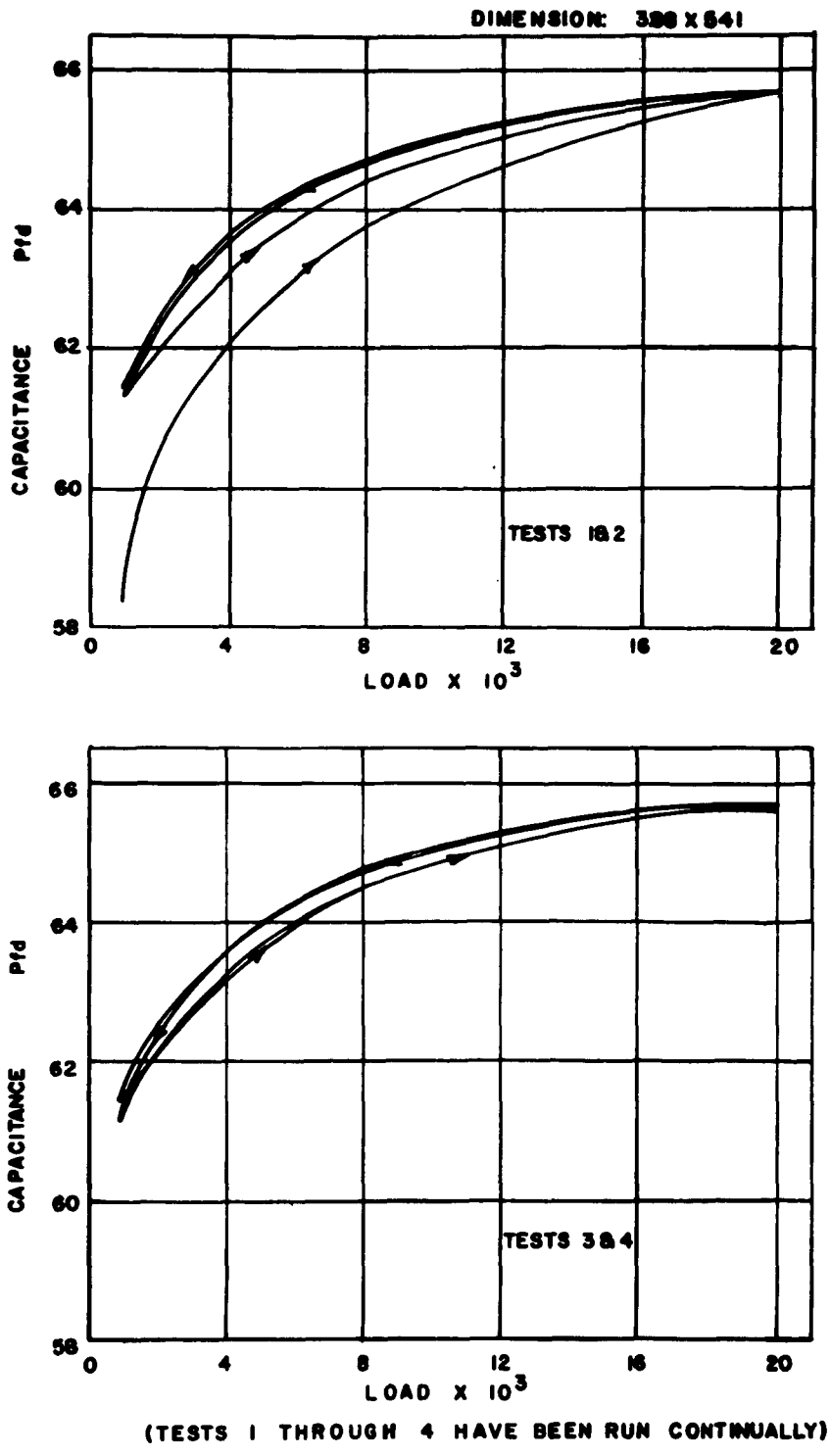

FIGURE 24. EFFECT OF LOAD ON THE CAPACITANCE BEHAVIOR OF POLYCRYSTALLINE ALUMINUM

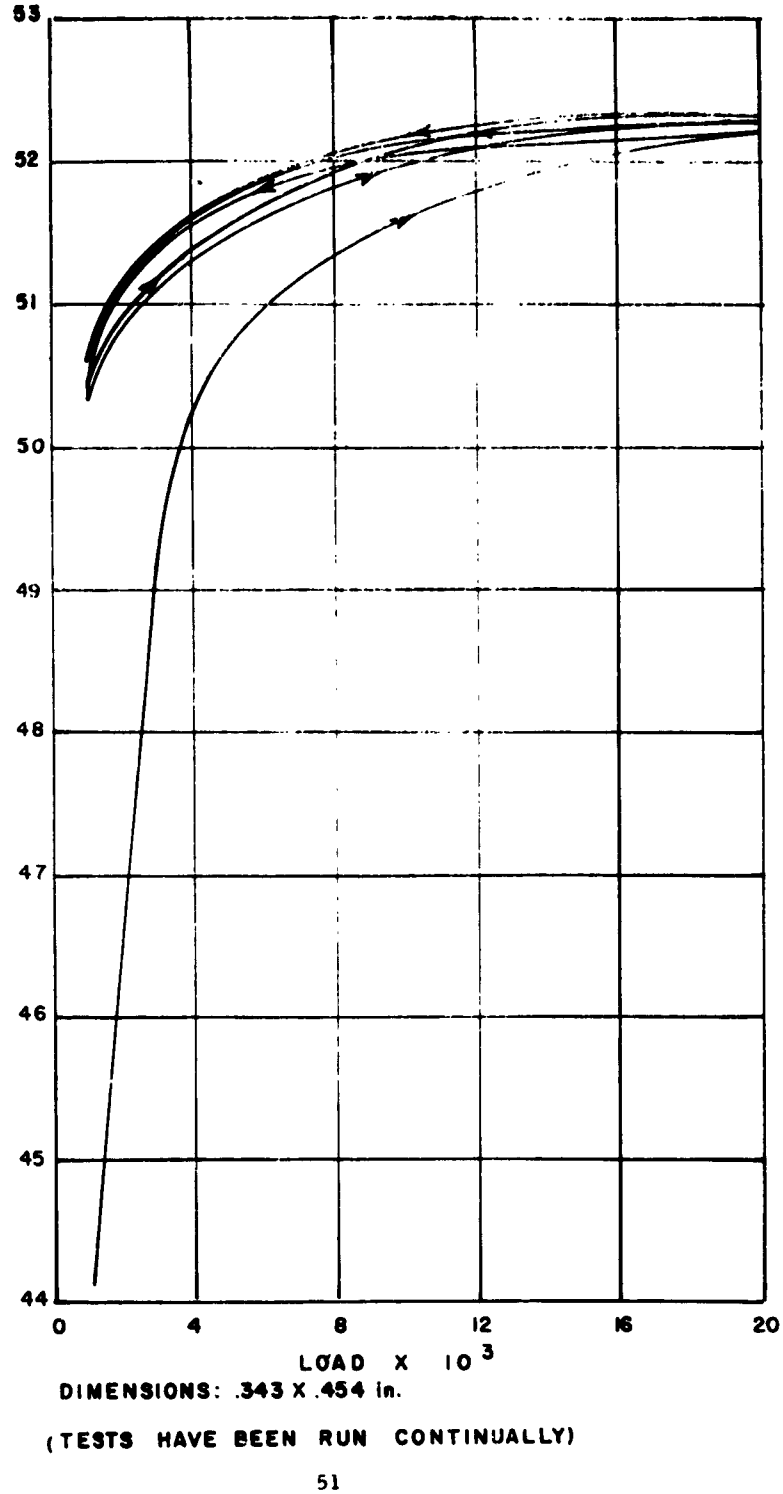

FIGURE 25. EFFECT OF LOAD ON THE CAPACITANCE BEHAVIOR OF POLYCRYSTALLINE ALUMINUM

Aeronautical Systems Division, Dir/Materials and Processes, Metals and Ceramics Lab, Wright-Patterson AFB, Ohio.
Rpt No. ASD TR 61-436, Pt I. NONDESTRUCTIVE ANALYSIS OF THE BRITTLE FRACTURE BEHAVIOR OF CERAMIC MATERIALS. Final report, Feb 63, 51pp. incl illus., tables, 62 refs.
Unclassified Report

A literature survey of theoretical and experimental approaches to brittle fracture was directed toward a nondestructive evaluation point of view. Surface decorating techniques were investigated.
A technique for calculating maximum stress

(over)

in an elastic loop was developed and applied to the measurement of the strength of glass fibers from three to seven mils in diameter. The strength values were related to surface condition by surface decoration techniques. Surface flaw decoration of cleaned and polished surfaces was performed by condensation of water on the surface. Minute flaws estimated to be less than 1000 Å deep were easily revealed.
Capacitance behaviors of polycrystalline materials were studied. Residual stress effects were observed under statically loaded conditions.

1. Nondestructive analysis
2. Ceramic materials
I. AFSC Project 7360, Task 736002
II. Contract No. AF 33(616)-7347
III. Mississippi State University, State College, Miss.
IV. J. H. Lauchner, T. F. Torries, J. L. Pentecost
V. Aval fr OTS
VI. In ASTIA collection

Aeronautical Systems Division, Dir/Materials and Processes, Metals and Ceramics Lab, Wright-Patterson AFB, Ohio.
Rpt No. ASD TR 61-436, Pt I. NONDESTRUCTIVE ANALYSIS OF THE BRITTLE FRACTURE BEHAVIOR OF CERAMIC MATERIALS. Final report, Feb 63, 51pp. incl illus., tables, 62 refs.
Unclassified Report

A literature survey of theoretical and experimental approaches to brittle fracture was directed toward a nondestructive evaluation point of view. Surface decorating techniques were investigated.
A technique for calculating maximum stress

(over)

in an elastic loop was developed and applied to the measurement of the strength of glass fibers from three to seven mils in diameter. The strength values were related to surface condition by surface decoration techniques. Surface flaw decoration of cleaned and polished surfaces was performed by condensation of water on the surface. Minute flaws estimated to be less than 1000 Å deep were easily revealed.
Capacitance behaviors of polycrystalline materials were studied. Residual stress effects were observed under statically loaded conditions.

1. Nondestructive analysis
2. Ceramic materials
I. AFSC Project 7360, Task 736002
II. Contract No. AF 33(616)-7347
III. Mississippi State University, State College, Miss.
IV. J. H. Lauchner, T. F. Torries, J. L. Pentecost
V. Aval fr OTS
VI. In ASTIA collection